# Energy-autonomous On-rotor RPM Sensor Using Variable Reluctance Energy Harvesting

**Conference Paper** · June 2019

DOI: 10.1109/IWASI.2019.8791251



**5 authors**, including:

Ye Xu
Mid Sweden University
**3** PUBLICATIONS **6** CITATIONS
SEE PROFILE

Sebastian Bader
Mid Sweden University
**29** PUBLICATIONS **104** CITATIONS
SEE PROFILE

Michele Magno
ETH Zurich
**169** PUBLICATIONS **2,560** CITATIONS
SEE PROFILE

Philipp Mayer
ETH Zurich
**13** PUBLICATIONS **59** CITATIONS
SEE PROFILE

# Energy-autonomous On-rotor RPM Sensor Using Variable Reluctance Energy Harvesting

Ye Xu*, Sebastian Bader*, Michele Magno†, Philipp Mayer† and Bengt Oelmann*
*Department of Electronics Design, Mid Sweden University, Sweden
†Department of Information Technology and Electrical Engineering, ETH Zurich, Switzerland
Email: ye.xu@miun.se

***Abstract*—Energy-autonomous wireless sensor systems have the potential to enable condition monitoring without the need for a wired electrical infrastructure or capacity-limited batteries. In this paper, a robust and low-cost energy-autonomous wireless rotational speed sensor is presented, which harvests energy from the rotary motion of its host using the variable reluctance principle. A microelectromechanical system (MEMS) gyroscope is utilized for angular velocity measurements, and a Bluetooth Low Energy System-on-Chip (SoC) transmits the acquired samples wirelessly. An analysis on the individual subsystems is performed, investigating the output of the energy transducer, the required energy by the load, and energy losses in the whole system. The results of simulations and experimental measurements on a prototype implementation show that the system achieves energy-autonomous operation with sample rates between 1 to 50 Hz already at 10 to 40 rotations per minute. Detailed investigations of the system modules identify the power management having the largest potential for further improvements.**

***Index Terms*—Energy harvesting, variable reluctance, energy-autonomous sensors, inertial RPM measurement**

## I. Introduction

With advancements in sensing, processing and communication technologies, industrial condition monitoring gains in popularity, enabling smart industrial machines and components [1]. Rotating parts are omnipresent in industrial applications, making their monitoring an essential task. Enabled by wireless communication technologies, sensing can be performed directly on the rotating object, providing data on, for example, rotational speed [2], [3].

Due to the fundamental difficulty of a wired power supply on rotating parts and the capacity and lifetime limitations of batteries, energy harvesting poses a competitive approach for supplying on-rotor electronic systems with the energy they require. Despite the growing research volume in energy harvesting [4], [5], experiences from end-to-end energy harvesting system designs are still limited.

In this paper, we report on the design, implementation and analysis of an energy-autonomous on-rotor RPM sensor system. The system uses a MEMS gyroscope for the measurement of the rotor's angular velocity and reports the acquired data wirelessly. The sensor system is powered by a variable reluctance energy harvester (VREH), exploiting the relative motion between the rotor and a stator based on electromagnetic induction. The system is particularly designed for applications with low rotational speeds of large-diameter shafts, making the utilization of standard electromagnetic generators infeasible. Moreover, the system includes a power management unit, coupling the energy transducer and the load.

This work was financially supported by the Knowledge Foundation through fund ASIS 20140323 and by VINNOVA through grant 2017-03725.

With the overall aim to analyze the end-to-end implementation of the on-rotor RPM sensor system, we investigate the performance of each sub-module, as well as the performance of a full prototype implementation. As a result, the key contributions of this paper are: (i) an energy-autonomous RPM sensor design, outperforming previously reported solutions; (ii) an end-to-end energy harvesting system implementation, investigating generated and required energy levels by the energy transducer and load, respectively; and (iii) an analysis of limitations in the system, identifying opportunities for further system optimizations.

Previously reported energy harvesting RPM sensor systems include the works by Parthasarathy et al. [6], and Buccolini and Conti [7]. In [6], the authors utilize a commercial variable reluctance transducer in order to implement an autonomous wheel speed sensor for automotive applications. The wheel speed sensor acts as an energy transducer to the wireless acquisition unit and a theoretical output power of $1\,\mathrm{mW}$ at $300\,\mathrm{rpm}$ is estimated. The authors, however, do not perform a detailed analysis of available power levels in the system, nor report achievable sample rates at different operating conditions. In [7], a self-powered wheel speed sensor for bicycles is proposed, utilizing an electromagnetic transducer based on the relative motion of a coil and magnets. The authors investigate the performance of the transducer, power management, and sensor systems. The measurement of rotational speed, however, is limited in resolution by the event-based implementation, generating pulses only on full rotations. Moreover, the proposed system generates sufficient power levels only at relatively high rotational speeds. In contrast to the previous work, we utilize an inertial rotational speed measurement, aiming at an accurate and energy-autonomous operation already at low rotational speeds, i.e., $10\,\mathrm{rpm}$ to $60\,\mathrm{rpm}$.

## II. System Design and Implementation

A system overview of the proposed energy-autonomous, on-rotor RPM sensor is depicted in Fig. 1. The system follows a common architecture for a wireless sensor node, containing

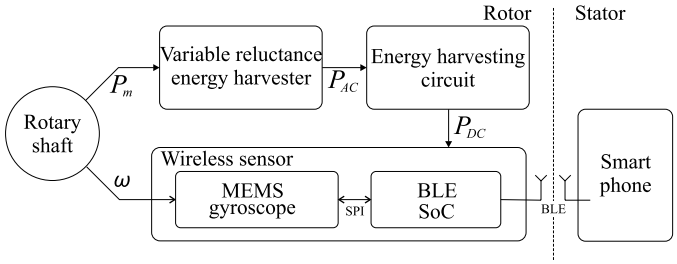


Fig. 1. Overview of the energy-autonomous on-rotor RPM sensor design, where $P_{\mathrm{M}}$ is the mechanical power, $P_{\mathrm{AC}}$ is the alternating current electrical power, $P_{\mathrm{DC}}$ is the direct current electrical power, and $\omega$ is the rotating speed of the rotary shaft.

a control/computation unit, a radio transceiver, and a sensing unit. In order to make the sensor system self-powered, moreover, the system includes a kinetic energy transducer that utilizes the rotary motion of the monitored host, as well as an energy harvesting conversion unit that adjusts the transducer's output to the load requirements.

### A. Wireless RPM Sensor

The core of the wireless RPM sensor design is a MEMS gyroscope, implementing an inertial approach to the measurement of rotational speed. Due to their integration and mass production, MEMS gyroscopes are highly competitive with respect to cost, size and power consumption. They, moreover, have a number of advantages over traditional event-based solutions (e.g., optical or magnetic encoders), which do not scale well to large shaft-diameters and low rotation rates. A closer investigation of the performance of MEMS gyroscopes can be found in [8], suggesting competitive performances to traditional approaches at much lower costs. In this system, a Bosch BMG-250 has been selected for the implementation, due to its small physical footprint ($2.5\,\mathrm{mm} \times 3.0\,\mathrm{mm}$) and low current draw in operation ($850\,\mu\mathrm{A}$).

The gyroscope is connected to a Rigado BMD-350 SoC, integrating an ARM microcontroller and a Bluetooth Low Energy (BLE) wireless transceiver. The angular velocity values of the axis aligned to the rotation direction are read out in digital format through a high-speed SPI bus. The sensor data is then wirelessly transmitted using the BLE transceiver.

### B. Variable Reluctance Energy Harvester

Utilizing inertial forces for the RPM measurement, the wireless sensor is mounted directly on the rotating object. Consequently, electrical energy needs to be provided to all active components on the rotor. The conversion of kinetic energy from the rotating object is a desirable alternative to a capacity-limited solution such as batteries. In the proposed system, an electromagnetic approach based on the variable reluctance principle is used. A variable reluctance energy harvester (VREH) exploits the relative movement between a pickup unit, containing a coil and magnets, and a ferromagnetic structure that affects the system's reluctance (e.g., a toothed wheel).

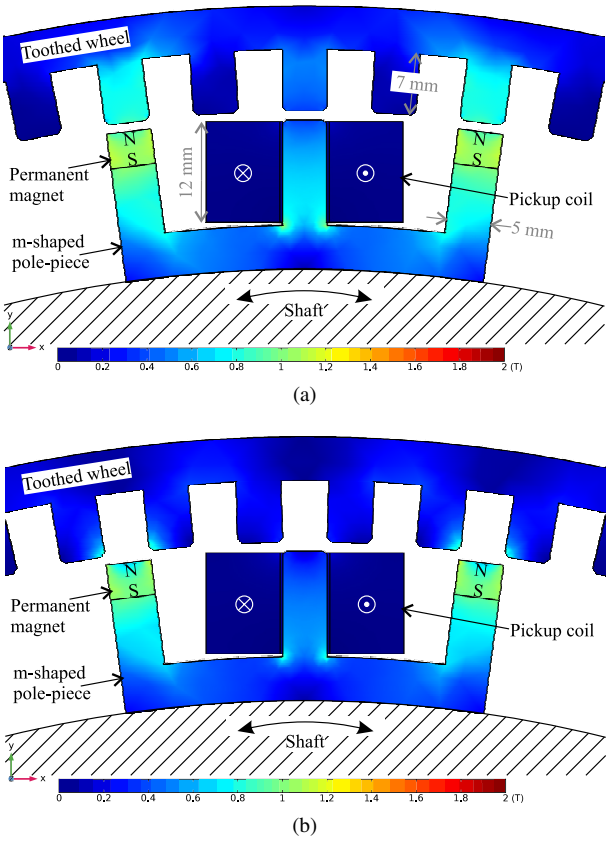


Fig. 2. Magnetic flux density distribution of the VREH topology at the two extreme positions, (a) aligned position and (b) unaligned position.

Figure 2 illustrates the on-rotor VREH structure applied in this work, demonstrating the magnetic flux distribution in its two extreme positions. The utilized pickup unit has an m-shape with two permanent magnets and a center coil, which has previously been demonstrated to outperform other pickup unit structures [9]. The rotation of the shaft results in a periodic arrangement variation between aligned position (Fig. 2a) and unaligned position (Fig. 2b). As a result of the varying reluctance, a magnetic flux change occurs in the core of the coil, inducing an alternating voltage according to Faraday's law.

By connecting an impedance matched load (i.e., $Z_{\mathrm{Coil}} = Z^*_{\mathrm{Load}}$) to the pickup coil, maximum power can be transferred to the load. The power level is a function of multiple system parameters and operating conditions and can be estimated according to [9] as

$$P_{\mathrm{L}} = \frac{N^2_{\mathrm{Coil}}}{8R_{\mathrm{Coil}}}\Delta^2_{\phi}\left[\frac{\omega N_{\mathrm{tooth}}}{2\pi}\right]^2. \tag{1}$$

Herein $P_{\mathrm{L}}$ is the output power at the matched load, $N_{\mathrm{Coil}}$ is the number of coil turns, $\Delta_{\phi}$ is the magnetic flux difference between aligned and unaligned positions, $\omega$ is the angular velocity, and $N_{\mathrm{tooth}}$ refers to the number of teeth in the toothed wheel. Neglecting the inductive part of the coil's impedance, an accurate estimation is only achieved at low operation frequencies.

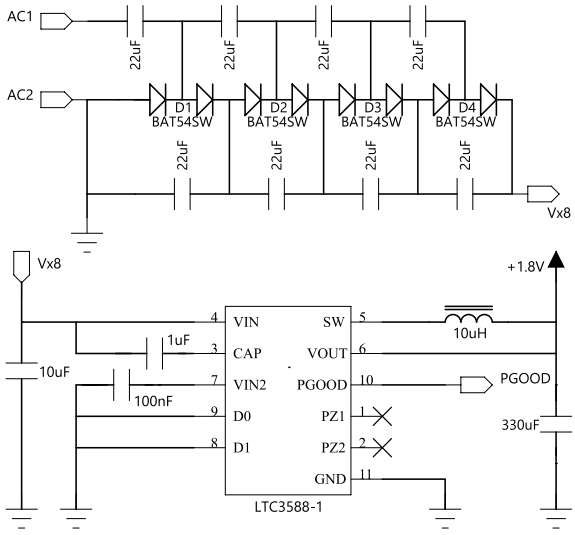


Fig. 3. Schematic overview of the energy harvesting conversion circuit, containing a four-stage Cockroft-Walton voltage multiplier and an LTC3588-1.

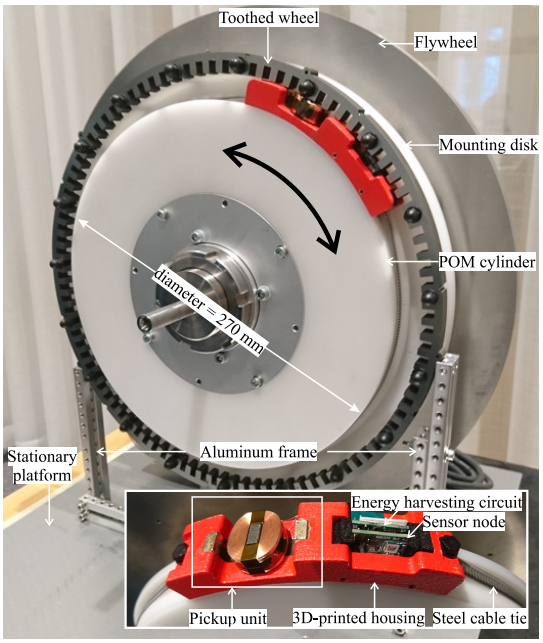


Fig. 4. Experimental setup generating the conditions of a low-speed, large-shaft rotating machine. A close-up of the mounted sensor system is provided in the inset.

### C. Electrical Conversion

Due to the AC output of the VREH unit, an electrical conversion module implementing AC-DC conversion is required. The conversion module is designed around a commercial energy harvesting integrated circuit, namely Analog Devices LTC3588-1. This device provides low quiescent consumption and high efficiency at relatively low output currents.

Although the LTC3588-1 allows for direct AC inputs through an internal bridge rectifier, an external rectification based on a four-stage Cockroft-Walton voltage multiplier [10] is implemented. This is motivated based on the relatively low voltages generated by the VREH transducer, as well as the high voltage drop over the bridge rectifier. The four-stage voltage multiplier rectifies the AC voltage and results in a DC voltage with an 8-fold multiplication. It thus enables operation even at low angular velocities, lifting the VREH output voltage to a range compatible with the LTC3588-1 input requirements (i.e., $2.7\,\mathrm{V}$ to $20\,\mathrm{V}$). While a pickup coil with a larger number of turns could be used as an alternative, this approach would result in a significantly larger space occupation and an increased coil resistance.

A schematic view of the power management module design is shown in Fig. 3. The output of this module is a stable $1.8\,\mathrm{V}$ DC supply to the wireless sensor.

## III. Experimental Setup

The wireless sensor is specifically designed for the purpose of monitoring angular velocity in low-speed and large-shaft rotating machines. Examples of such applications include feeders and drums in the cement industry, drives in food and mining industries, mixers and roll mills in the rubber and plastic industries, as well as heavy machines such as cranes, excavators, and wind turbines [8], [11].

In this paper, the specific requirements of large-scale hydraulic motors for industrial applications are used to investigate the system performance. As a result, a shaft diameter of $270\,\mathrm{mm}$ has been chosen, and evaluations are conducted under low rotational speed in the range of $10\,\mathrm{rpm}$ to $60\,\mathrm{rpm}$.

Figure 4 depicts the experimental setup, containing a polyoxymethylene (POM) cylinder that emulates the system's rotating shaft. The POM cylinder is driven by a controllable DC motor, operating at low rotational speeds. A toothed wheel made of electric steel is mounted on a stationary mounting disk. The on-rotor unit integrates the wireless sensor node, the energy harvesting conversion circuit, and the VREH pickup unit, being enclosed in a 3D-printed housing and fixed on the rotor surface. The setup creates a mechanical air gap of $1\,\mathrm{mm}$ between the pickup unit and toothed wheel. Moreover, a flywheel is mounted onto the POM cylinder in order to maintain a stable rotation speed and smooth speed transitions.

The pole-piece and toothed wheel are laminated structures stacked by 28-layers of electrical steel NSC-35H230, resulting in a stack depth of $10.15\,\mathrm{mm}$. Two N50-NdFeB permanent magnets provide the constant MMF in the pickup unit, and are glued on the pole-piece. The pickup coil is wound on the center pole of the pole-piece, and its two terminals are connected to the conversion circuit board (*AC1* and *AC2*, as shown in Fig. 3).

For simplicity, we configure the BLE SoC to operate in a beacon mode to transmit the payload in advertisement packages. Consequently, this configuration requires no scan response from the smartphone. The transmission power of the BLE transceiver is set to $-20\,\mathrm{dBm}$, resulting in a low power consumption while transmitting to a nearby operator.

TABLE I
DURATION AND ENERGY CONSUMPTION OF WIRELESS SENSOR STATES

| State | Description | Time (ms) | Energy ($\mu$J) | Contribution (%) |
|---|---|---|---|---|
| SPI-wu | Sensor wakeup | 0.24 | 1.33 | 1.6 |
| S-init | Sensor initialization | 32.48 | 25.89 | 31.3 |
| S-meas | Sensor measurement | 27.32 | 37.78 | 45.6 |
| SPI-tx | Sensor readout | 0.25 | 1.53 | 1.8 |
| BLE | BLE transmission | 3.73 | 16.26 | 19.7 |
| Total | | 64 | 82.79 | |

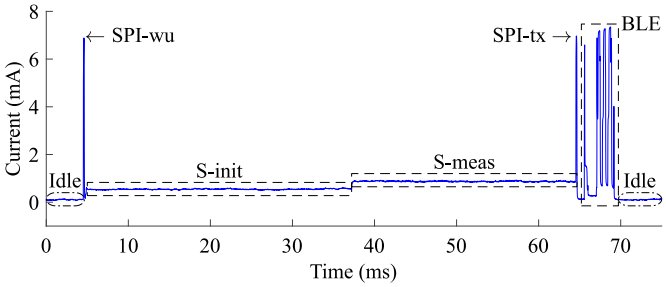


Fig. 5. Current profile for the acquisition of one sample on the wireless sensor. The total duration of a sample acquisition is 64 ms.

The transmitted payload is the sensor data, consisting of two 16-bit readings (i.e., one for angular velocity, and one for temperature).

## IV. System Evaluation

The evaluation of the system is conducted in two steps. Firstly, the performance of each module is evaluated individually in order to provide a better understanding of available energy, required energy, and losses in the system. Secondly, the system is integrated into a full system prototype, providing measures of the overall system performance.

### A. Wireless Sensor Energy Consumption

The energy consumption of the wireless sensor defines the required energy to be generated for correct system operation. Operating at a constant supply voltage of $1.8\,\mathrm{V}$, the energy consumption can be deducted from current measurements. The current profile of the wireless sensor has been acquired, measuring the voltage drop over a $1.068\,\Omega$ low-side shunt resistor. The measurements have been performed with a Keysight MSOX3024T oscilloscope in differential mode.

Figure 5 shows the current profile for a sample acquisition of the wireless sensor, annotating key phases in the process. The total sampling period is $64\,\mathrm{ms}$ long, with the highest power demands posed by the BLE SoC. Table I lists the individual phases together with their time and energy requirements. From this table it becomes obvious that it is the gyroscope that dominates the energy footprint (i.e., about $77\,\%$), despite its low power demand. With approximately $83\,\mu\mathrm{J}$, the overall energy footprint of a single sample is low.

In addition, the current draw of the wireless sensor during idle state is approximately $5\,\mu\mathrm{A}$. At low duty cycles, this idle current results in a significant contribution to the overall energy need, whereas its impact reduces dramatically at the higher sampling intervals targeted for this system.

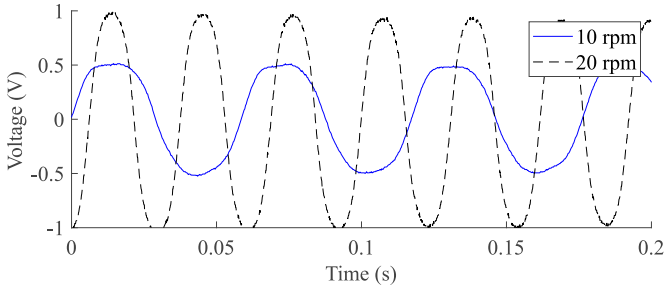


Fig. 6. Output voltage measurement of the pickup coil over an impedance matched load at $10\,\mathrm{rpm}$ and $20\,\mathrm{rpm}$, respectively. Differences in output amplitude and frequency can be observed.

### B. VREH Performance

In order to evaluate the performance of the VREH, its output power under different operating conditions can be used as a metric. Under ideal conditions, the attached load is impedance matched to the VREH transducer, maximizing the power transfer between source and load. Due to the relative low frequencies of interest in this study, the impedance matching condition can be simplified to $R_{\mathrm{Coil}} = R_{\mathrm{Load}} = 180.5\,\Omega$.

Figure 6 shows the output voltages of the VREH under two rotating speeds and with matched resistive load. It can be seen that with changing angular velocity, both amplitude and frequency of the output voltage are affected. The ideal output power in these scenarios can be estimated based on the RMS voltage and the load condition, such that

$$P_{\mathrm{out}} = V_{\mathrm{RMS}}^2 / R_{\mathrm{Load}}\,. \tag{2}$$

Already at $10\,\mathrm{rpm}$, for example, the RMS output voltage is $405\,\mathrm{mV}$, resulting in an output power of approximately $910\,\mu\mathrm{W}$. This theoretically enables for a sample rate of $10\,\mathrm{Hz}$.

Figure 7, moreover, depicts how the output power of the VREH scales with increasing rotational speed. The results in this figure are obtained through three-dimensional finite element simulations conducted in COMSOL Multiphysics. The simulation results are experimentally verified in the range of rotation speeds compatible with the experimental setup (see Section III), demonstrating a good match between simulations and experiments. In the observed range, the output power follows a roughly linear dependency with the rate of rotation, leading to almost $15\,\mathrm{mW}$ at $60\,\mathrm{rpm}$. The linear relationship is a consequence of impedance mismatch at higher rotational speeds, neglecting the imaginary part of the impedance. For reference purposes, the theoretical output under true impedance matching is included in the figure.

### C. Conversion Efficiency

As previously described in Section II-C, an AC-DC conversion subsystem is required to provide a stable DC voltage to the load. This subsystem inevitably consumes a portion of

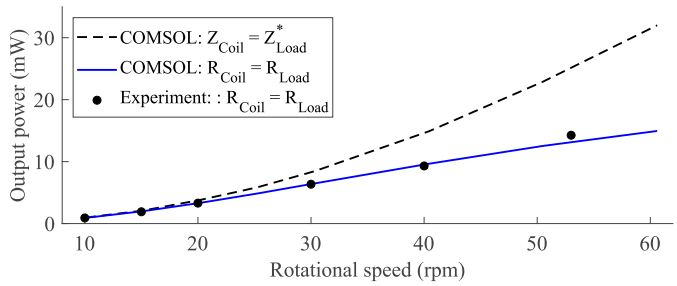


Fig. 7. Average output power of the VREH at different rotational speeds. Comparison between resistive and complex conjugate matching demonstrates little influence below 20 rpm.

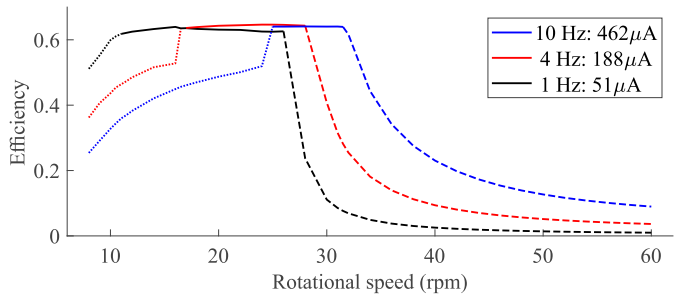


Fig. 8. Power conversion efficiency of the energy harvesting conversion circuit for three sampling frequencies of the wireless sensor at different rotating speeds.

the harvested energy, which can be expressed as its conversion efficiency. The expected efficiency of the commercial energy harvesting IC (LTC3588-1) is well described in the device datasheet. In this design, however, an additional rectification stage has been added, affecting the overall conversion efficiency.

In order to evaluate the overall efficiency of the conversion module, SPICE simulations have been performed containing both the voltage multiplier and the LTC3588-1. The SPICE simulations use a voltage source as input, implementing the specific properties of the VREH transducer. Exemplar results of these simulations are shown in Fig. 8, providing the overall conversion efficiency as a function of the rotational speed for a selection of sample rates (i.e., load currents). It is noteworthy to remember that a change in rotational speed leads to different amplitudes and frequencies of the input AC voltage. In the depicted range the input voltages (peak) range from approx. 1 V to 5 V, with frequencies from approx. 20 Hz to 100 Hz.

Figure 8 shows three distinct phases for each sample rate case. The dotted part at low rotational speeds indicates input conditions insufficient to lead to a stable output voltage of 1.8 V. The second, solid part indicates normal operation, where the overall conversion efficiency is stable at approx. 61.5 %. Finally the dashed part at higher rotational speeds demonstrates the effect of input protection, in which a Zener diode guarantees not to exceed the max. input voltage to the LTC3588-1. The start and end conditions for certain phases can be affected by the implementation of the voltage

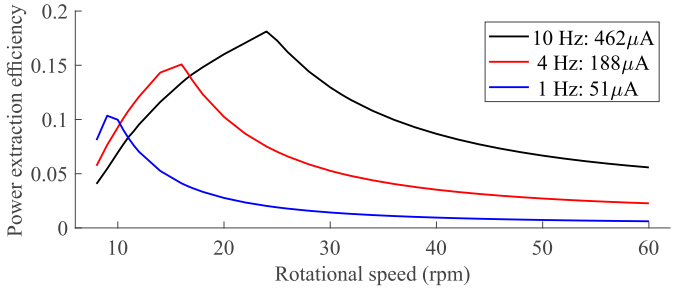


Fig. 9. Power extraction efficiency as a function of rotational speed for different sampling frequencies of the wireless sensor.

multiplier, but a widely applicable solution is difficult to be achieved with this architecture.

### D. Full System Evaluation

Finally, the full system performance is evaluated, considering the performance of each subsystem, as well as their interaction. A figure of merit suitable for the system evaluation is the power extraction efficiency (PEE), which describes the ratio of available power to the load with respect to the ideally extractable power from the transducer [12].

Figure 9 shows the estimated PEE of the full system as a function of rotational speed, and for a selection of sampling rates. The results in this figure originate from SPICE simulations of the system implementation. For the PEE, in this regards, two main contributions can be identified. On the one hand, the PEE is affected by the conversion efficiency presented in Section IV-C. On the other hand, connecting the conversion subsystem to the transducer leads to an impedance mismatch, reducing the extracted power as compared to the ideal condition presented in Fig. 7.

The main reason for the impedance mismatch is the large equivalent capacitance of the Cockroft-Walton voltage multiplier. This capacitance could ideally be compensated for by an additional series inductance, but the large values required make an implementation unrealistic. Figure 9, moreover, shows that the PEE is dependent on the rotational speed, providing an optimum operating condition for each load condition.

In order to investigate what effect the available power has on the wireless sensor scenario, the achievable sample intervals are evaluated as a function of the rotational speed. This investigation takes the entire system into account. The results of this analysis are shown in Fig. 10, with the solid curve being a result of the ideal VREH output power, the PEE of the system, and the load requirements presented in Section IV-A. Moreover, this estimation is confirmed by an experimental verification at a set of different rotational speeds.

With increasing output power at increasing rotational speed, the sample interval decreases as a function of rotational speed. However, the sample interval is not only limited by the available power, but also by timing restrictions of the wireless sensor. Consequently, four distinct phases have been indicated in the figure. Phase (a) indicates normal operation according to the sampling sequence as illustrated in Fig. 5. In this operation,

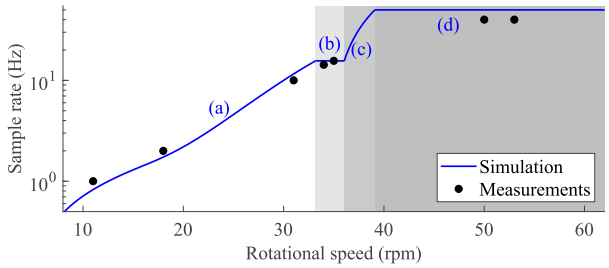


Fig. 10. Estimated sample frequency of the wireless sensor at different rotating speeds

the sample acquisition takes approx. 64 ms. At approx. 33 rpm (start of phase (b)), enough energy is harvested to continuously acquire samples, leading to the maximum sampling frequency of 15.625 Hz in this operating mode.

In order to reach a higher sampling frequency, the operating mode has to be changed. This can be achieved by maintaining the gyroscope in active mode, avoiding its initialization and reducing its readout time. This operating mode will require a higher average power, which is available from approx. 36 rpm and onward. In phase (c), thus, a further reduction of the sample interval with increasing rotational speed can be observed. Finally, phase (d) is reached at approx. 39 rpm. At this point, both gyroscope and BLE transceiver can operate continuously. As a result, the sample interval is limited by the maximum advertisement interval of 20 ms for the BLE communication. Further improvements of sample rates are only possible if switching to a connection-based operation.

Figure 10, moreover, shows that a sample rate higher that 1 Hz is obtained already at approx. 12 rpm. The experimental data shows that this sample rate can be achieved even at slightly lower rotational speeds, at approx. 11 rpm.

## V. Conclusion

In this paper, we designed, implemented and analyzed an energy-autonomous, on-rotor sensor system using variable reluctance energy harvesting. The wireless sensor monitors the angular velocity and temperature of a low-speed and large-diameter rotary structure, without the need for a wired power supply or battery. The compact design, including a low-cost MEMS gyroscope and a robust electromagnetic energy harvesting system, is suitable for industrial and cost-sensitive applications.

The results from simulations and a prototype implementation demonstrate that the VREH approach can enable autonomous operation of the wireless sensor already at low rotational speeds. A sample rate of 1 Hz, including sensor initialization, readout, and wireless transmission via BLE, requires approx. 90 µJ. The required power level for this is made available to the load already at 11 rpm.

An investigation of the individual subsystems provides an understanding of the required energy by the wireless sensor; the extractable energy from the VREH transducer under different operating conditions; and the efficiency of the system through conversion losses. Combining the individual modules into a full system prototype, furthermore, demonstrates additional losses due to mismatches in module impedances. As a result, we show that it is the energy harvesting conversion circuit that has a large influence on the power delivery to the load. With power extraction efficiencies below 20 %, a considerable portion of energy that could potentially be harvested by the system is lost. Particularly, impedance matching would help to improve the PEE, but is difficult to be achieved for the utilized conversion circuit implementation, due to the large equivalent capacitance of the voltage multiplier.

For further improvement, thus, an alternative implementation of the electrical conversion is the primary target to be addressed. Besides improving the impedance match between transducer and the conversion circuitry, an AC-DC conversion with high efficiency over a wider operating range would be desirable. In addition, further optimizations on the VREH transducer can be performed, not only improving its output power, but even optimizing for an overall higher PEE.

Nonetheless, we demonstrated that the proposed system design reaches the maximum achievable sample frequency of the underlying technology (i.e., 50 Hz) already at low rotational speeds below 50 rpm.

## References


[1] A. R. Mohanty, *Machinery Condition Monitoring: Principles and Practices*. CRC Press, 2018.

[2] C. Schantz, K. Gerhard, J. Donnal, J. Moon, B. Sievenpiper, S. Leeb, and K. Thomas, "Retrofittable Machine Condition and Structural Excitation Monitoring From the Terminal Box," *IEEE Sensors Journal*, vol. 16, no. 5, pp. 1224–1232, Mar 2016.

[3] Y. Cheng, Z. Wang, and W. Zhang, "A Novel Condition-Monitoring Method for Axle-Box Bearings of High-Speed Trains Using Temperature Sensor Signals," *IEEE Sensors Journal*, vol. 19, no. 1, pp. 205–213, Jan 2019.

[4] A. S. Weddell, M. Magno, G. V. Merrett, D. Brunelli, B. M. Al-Hashimi, and L. Benini, "A Survey of Multi-source Energy Harvesting Systems," in *Design, Automation Test in Europe Conference Exhibition (DATE)*, Mar 2013, pp. 905–908.

[5] M. Magno, L. Spadaro, J. Singh, and L. Benini, "Kinetic Energy Harvesting: Toward Autonomous Wearable Sensing for Internet of Things," in *International Symposium on Power Electronics, Electrical Drives, Automation and Motion (SPEEDAM)*, Jun 2016, pp. 248–254.

[6] D. Parthasarathy, P. Enoksson, and R. Johansson, "Prototype Energy Harvesting Wheel Speed Sensor for Anti-lock Braking," in *Proceedings of IEEE International Symposium on Robotic and Sensors Environments*, Nov 2012, pp. 115–120.

[7] L. Buccolini and M. Conti, "An Energy Harvester Interface for Self-Powered Wireless Speed Sensor," *IEEE Sensors Journal*, vol. 17, no. 4, pp. 1097–1104, Feb 2017.

[8] M. S. Mustafa, P. Cheng, and B. Oelmann, "Stator-Free Low Angular Speed Sensor Based on a MEMS Gyroscope," *IEEE Transactions on Instrumentation and Measurement*, vol. 63, no. 11, pp. 2591–2598, Nov 2014.

[9] Y. Xu, S. Bader, and B. Oelmann, "A Survey on Variable Reluctance Energy Harvesters in Low-Speed Rotating Applications," *IEEE Sensors Journal*, vol. 18, no. 8, pp. 3426–3435, Apr 2018.

[10] I. C. Kobougias and E. C. Tatakis, "Optimal Design of a Half-Wave Cockcroft - Walton Voltage Multiplier With Minimum Total Capacitance," *IEEE Transactions on Power Electronics*, vol. 25, no. 9, pp. 2460–2468, Sep 2010.

[11] L. Song, H. Wang, and P. Chen, "Vibration-Based Intelligent Fault Diagnosis for Roller Bearings in Low-Speed Rotating Machinery," *IEEE Transactions on Instrumentation and Measurement*, vol. 67, no. 8, pp. 1887–1899, Aug 2018.

[12] K. D. Ngo, A. Phipps, T. Nishida, J. Lin, and S. Xu, "Power Converters for Piezoelectric Energy Extraction," in *ASME International Mechanical Engineering Congress and Exposition*, 2006, pp. 597–602.